Layer-Wise Transfer Learning and Deep Fine-Tuning for Multi-Class Brain Tumour Classification Using MRI Images

Pillareddy Vamsheedhareddy[1], Tippani Gayathri[2], Ch Rathan Kumar[3], P Bala Krishna[4]

[1,2] Assistant Professor, Department of CSE-AIML, Keshav Memorial Engineering College, Kachavanisingaram, Uppal, Hyderabad, Telangana, India.

[3,4]Assistant Professor, Department of CSE-AIML, Keshav Memorial Engineering College, Kachavanisingaram, Uppal, Hyderabad, Telangana, India

ABSTRACT

Accurate and timely identification of brain tumours is a decisive factor in effective clinical treatment and improved patient survival. Magnetic Resonance Imaging (MRI) serves as a crucial non-invasive modality for visualising tumour morphology; however, manual interpretation of MRI scans is both time-consuming and subject to inter-observer variability. To address these limitations, this study investigates the effectiveness of deep learning-based automated classification using three distinct variants of the DenseNet201 architecture for multi-class brain tumour recognition. The models are designed to categorise MRI images into four classes: glioma, meningioma, pituitary tumour, and normal (non-tumour). The first model, referred to as B-DenseNet201-CA, is trained entirely from random initialisation to establish a baseline performance. The second model, PT-DenseNet201-FB, adopts a transfer learning strategy by utilising a DenseNet201 network pretrained on ImageNet, where the convolutional backbone is frozen and only the classifier layers are trained. The third and most advanced approach, FT-DenseNet201-TL, performs selective fine-tuning by retraining the final 50 layers of the pretrained network to better adapt the learned representations to the medical imaging domain. All models are trained and evaluated on a publicly available brain MRI dataset using standard performance metrics, including accuracy, precision, recall, F1-score, and confusion matrices. Experimental results reveal that the baseline model achieves an accuracy of 74.11%, highlighting the difficulty of training deep networks from scratch on limited medical datasets. The frozen transfer learning model significantly improves classification performance, achieving an accuracy of 90.81%, thereby demonstrating the effectiveness of pretrained feature representations. The fine-tuned transfer learning model delivers the highest performance, attaining an accuracy of 94.18% and exhibiting improved class-level discrimination, particularly for visually similar tumour categories. The findings confirm that partial fine-tuning of a pretrained DenseNet201 architecture provides a computationally efficient and highly accurate solution for brain tumour classification. This work underscores the critical role of transfer learning in medical image analysis and suggests strong potential for integration into clinical decision-support systems to enhance diagnostic reliability and consistency.

Keywords: Brain Tumour Classification; Magnetic Resonance Imaging (MRI); DenseNet201; Transfer Learning; Deep Fine-Tuning; Convolutional Neural Networks; Medical Image Analysis; Multi-Class Classification; Radiomics; Tumour Subtype Identification

1. Introduction

It is very important to protect everyone's health because brain tumors cause a lot of cancer-related illness and death [1]. Accurately finding and classifying brain tumor groups is very important in clinical neuro-oncology because it helps doctors plan treatments and give each patient a personalized care. MRI is still the best imaging method because it provides high-resolution information on anatomy and function that is needed for alternative diagnosis and planning treatment [2]. Even though imaging tools and diagnostic methods are always getting better, it is still very hard to accurately classify brain tumor subtypes because their morphological features and histopathological differences are so similar [3].

While conventional radiological assessments effectively delineate tumor boundaries and assess localization [4], they often fall short in capturing subtle differences in tissue composition and molecular heterogeneity, which are crucial for accurate subtype determination [5]. This gap necessitates the development of advanced image analysis frameworks capable of extracting discriminative features and enhancing classification accuracy. The present study addresses this limitation by leveraging computational imaging techniques and radiomics-driven modeling to augment the interpretive capacity of MRI in the grouping of different types of brain tumors.

Even though cutting-edge designs like EfficientNet, ConvNeXt, and Vision Transformers (ViT) have shown they work better, in large-scale natural image classification tasks, their computational complexity and lack of interpretability pose barriers to clinical deployment. These models often require extensive computational resources and do not readily offer transparent reasoning behind predictions—an essential requirement in high-stakes medical decision-making. This study uses a custom CNN architecture to find the best mix between accuracy in prediction, ease of computation, and ease of understanding of the model. The proposed model is optimized for real-world clinical settings, particularly in resource-constrained environments, where explainability and trust in automated predictions are paramount for adoption by healthcare professionals.

In the past few years, medical image analysis based on DL has become a strong way to make diagnostic systems more accurate and faster, especially in difficult areas like classifying brain tumors. More and better annotated MRI datasets are becoming available, and CNNs have made big steps forward in automating the discovery and classification of tumor subtypes. However, despite these advancements, selecting the most appropriate architectural approach—whether to build a deep model from scratch, utilize transfer learning, or adopt a fine-tuning strategy—remains a challenge, especially when balancing generalization, interpretability, and computational efficiency. This study systematically explores three distinct variants of DenseNet201-based models for multi-class brain tumor classification: a baseline model trained from scratch, a transfer learning model with a frozen pretrained base, and a selectively fine-tuned pretrained model. The overarching objective is to evaluate the effectiveness of each approach in terms of accuracy, generalizability, and clinical applicability while highlighting their respective trade-offs in data-limited and resource-constrained medical settings.

The Objectives of the Study are

i. **To develop the Baseline DenseNet201 - Custom Architecture (B-DenseNet201-CA)** from scratch using TensorFlow/Keras, preserving the original DenseNet201 block structure, and evaluate its capability to classify multi-class medical images without pre-initialized weights.
ii. **To implement the Pretrained DenseNet201 with Frozen Base (PT-DenseNet201-FB)** by leveraging a DenseNet201 model pretrained on ImageNet, freezing the convolutional base, and training a custom classification head specific to the medical imaging task.
iii. **To enhance the adaptability of the pretrained model through Fine-Tuned Pretrained DenseNet201 (FT-PT-DenseNet201)**, involving selective unfreezing of the last 50 layers (excluding BatchNormalization) and re-training with a reduced learning rate to capture domain-specific features.
iv. **To perform a comprehensive comparative evaluation** of the three variants in terms of accuracy, generalization capability, class-wise performance (especially for meningioma and pituitary tumors), and overall model robustness on limited medical imaging data.

The article is structured in the following manner:

In Section 2, we talk about the connected work. In Section 3, the suggested implementation is laid out. The Results and Analysis of a Proposed Model can be found in Section 4. Section 5 is all about the and includes the end.

2. Related Work

Over the past two decades, medical image analysis has emerged as a critical area of research, particularly in applications related to brain tumor detection and diagnosis. This field has witnessed rapid advancements through the integration of ML and DL methodologies for interpreting MRI and CT scans, aiding in segmentation, classification, and visualization tasks.

Early studies in this domain leveraged ML-based techniques to classify brain images and understand structural anomalies [6]. Abd-Ellah et al. [7] offered a comprehensive comparison of traditional ML and DL models,

highlighting their advantages and limitations in MRI-based tumor diagnosis. Their follow-up study introduced a semi-automatic segmentation approach using T1W-configured 3D MRI [8], illustrating improved delineation of tumor regions. While CNNs have also been widely applied in other medical domains, such as breast cancer detection [9], their architecture design—especially in models like GoogLeNet, DenseNet201, AlexNet, and ResNet50—has shown strong performance in brain tumor classification as well [10].

Further advancements focused on enhancing segmentation precision. In [11], the authors looked into how to improve the segmentation accuracy of MR pictures using 3D CNNs, SVMs, and multi-class SVMs. In [12], a mixed method using deep feature extraction and regular classifiers was suggested. CNNs were used to get features, which were then fed into Naive Bayes, SVMs, and multilayer perceptrons. With SVM, the accuracy reached up to 96%. Kumar et al. [13] tried a number of ML and DL models and found that classic SVMs were 92.4% accurate and a five-layer CNN was 97.2% accurate. Khan et al. [14] also made a combination method that combined VGG19 and K-means clustering. This method was 94% accurate after preprocessing and statistical normalization.

Fusion strategies have also gained prominence. The authors in [15] proposed Using DenseNet for classification and custom 3D CNNs for segmentation on both 2D and 3D MRI images, we got 92% and 85% accuracy, respectively. Kang et al. [16] used a deep CNN ensemble and machine learning models. They discovered that SVM with radial basis function worked best. Another addition [17] showed that extreme gradient boosting can accurately tell the difference between CNS tumors up to 95% of the time. Also, in [18], a new group approach called Adaptive Fuzzy Deformable Fusion was introduced. It combines Fuzzy C-Means Clustering with deformable models to achieve 95% accuracy in classification.

Deep learning optimization has also been explored. Mehrotra et al. [19] evaluated CNNs such as AlexNet with various optimizers (Adam, RMSprop, SGD), identifying superior performance with appropriate calibration. Grampurohit and Shalavadi [20] applied a CNN-VGGNet hybrid model for classifying 253 MR images, reporting validation accuracies of 86% and 97% for custom and pre-trained models respectively. Preprocessing strategies such as global/adaptive thresholding and histogram equalization were discussed in [21], leading to 95% accuracy using a ResNet101 V2 via transfer learning.

Optimization algorithms have also contributed to model selection. A GA–CNN hybrid was proposed in [22], where the genetic algorithm autonomously selected the CNN architecture, enabling accurate detection of glioma, meningioma, and pituitary tumors with 90.9% to 94.2% accuracy. Majib et al. [23] introduced VGG-SCNet, a stacked classifier-based model fine-tuned on VGG-16, improving efficiency via data augmentation and sixth-layer feature extraction.

The role of image preprocessing in enhancing tumor localization has been emphasized in [24], while [25] demonstrated that multimodal fusion through CNNs enhances detection from 3D MRI. Comparative analyses of CNN architectures in [26] revealed that ResNet-50 outperformed GoogleNet and VGGNet, offering 96.5% accuracy with lower computational cost.

Additional studies reinforce the potential of non-conventional classifiers. Akkus et al. [27] applied random forest classifiers using handcrafted features for BraTS 2015 dataset segmentation. Pereira et al. [28] used deep CNNs for multi-type tumor classification with superior performance. The C-CNN strategy in [29] localized tumors using both local and global pathways, while nested CNN structures were explored in [30]. The BCM-CNN model, enhanced with a sine–cosine optimization strategy, was introduced in [31], and ensemble models with U-Net segmentation were analyzed in [32]. Complex segmentation was further addressed by the 3D-Dense-UNet model in [33], although challenges persist in computation and tumor-type generalization.

To counteract these limitations, [34] proposed a hybrid CNN and probabilistic neural network for improved segmentation, and [35] employed cascaded CNNs for multi-class segmentation. Nevertheless, many of these models remain data-intensive and struggle with unknown tumor types, requiring innovative solutions to improve generalizability and reduce training overhead [36].

2.1. Research Gaps and Their Addressal

Despite significant progress in deep learning-based brain tumor classification, several limitations continue to hinder the performance and practical deployment of existing models in clinical environments. Through an extensive review of current literature and empirical evaluation, the following research gaps have been identified:

Identified Research Gaps

i. **Lack of Domain Adaptation in Transfer Learning**
Most transfer learning models rely on frozen feature extractors trained on natural images, which restricts their ability to adapt to domain-specific variations in brain MRI data.

ii. **Overfitting in Models Trained from Scratch**
Deep architectures such as DenseNet and ResNet, when trained end-to-end on small-scale medical datasets, exhibit poor generalization and tend to overfit due to insufficient data volume.

iii. **Inadequate Performance on Complex Tumor Types**
Tumor subtypes like meningioma and pituitary, which have overlapping visual features, are often misclassified due to the lack of specialized high-level feature representation.

iv. **Imbalanced Evaluation Metrics**
Several studies report only overall accuracy, overlooking macro-averaged precision, recall, and F1-scores, which are critical in class-imbalanced medical classification tasks.

v. **Inefficient Use of Computational Resources**
Training deep networks from scratch requires substantial computational power and time, which is often impractical for clinical applications with limited infrastructure.

vi. **Lack of Two-Phase Learning Strategies**
Few studies adopt progressive learning paradigms—such as initial head training followed by selective fine-tuning—despite their known effectiveness in low-data regimes.

Although deep learning has made significant strides in the field of medical image classification, several critical research gaps remain unaddressed, particularly in the context of brain tumor subtype identification using MRI. This study identifies six key gaps and proposes two strategically designed model variants—Pretrained DenseNet201 with Frozen Base (PT-DenseNet201-FB) and Fine-Tuned Pretrained DenseNet201 (FT-PT-DenseNet201)—to bridge them effectively.

The first major gap lies in the limited domain adaptation capabilities of traditional transfer learning methods. Many approaches freeze the convolutional base pretrained on natural image datasets, which prevents the model from learning domain-specific representations relevant to brain MRI. While PT-DenseNet201-FB also follows this strategy, it highlights this limitation. In contrast, FT-PT-DenseNet201 addresses this issue by By unfreezing the first 50 layers of the pre-trained base, the model can react more deeply to the specific features of medical imaging data, which makes it more sensitive to those features.

Secondly, models trained from scratch on limited datasets often suffer from overfitting due to the high number of trainable parameters. PT-DenseNet201-FB effectively mitigates this issue by reducing the number of trainable weights during initial training, thus avoiding overfitting. FT-PT-DenseNet201 further enhances generalization by combining low learning rate fine-tuning with frozen Batch Normalization layers, which stabilizes internal covariate shifts during training.

A third gap is the inadequate performance of existing models on complex tumor types such as meningioma and pituitary, which often present with overlapping visual patterns. The rigid features learned in PT-DenseNet201-FB result in moderate accuracy for these classes. However, FT-PT-DenseNet201, through its selective fine-tuning strategy, demonstrates markedly improved class-wise F1-scores, achieving over 92% in all categories and showing significantly better differentiation of these challenging tumor subtypes.

Another recurring issue in prior work is the over-reliance on overall accuracy as the sole performance metric. This can be misleading in class-imbalanced datasets, where minority classes are underrepresented. Both PT-DenseNet201-FB and FT-PT-DenseNet201 incorporate balanced evaluation metrics, including macro-averaged precision, recall, and F1-scores. Notably, FT-PT-DenseNet201 achieves superior per-class and macro-level performance, offering a more reliable assessment of real-world applicability.

Furthermore, the computational inefficiency of deep CNNs poses a challenge for deployment in clinical environments. PT-DenseNet201-FB, by freezing the backbone, offers a lightweight and computationally efficient solution with fast training cycles. Although FT-PT-DenseNet201 introduces a slightly higher training load due to the additional fine-

tuning phase, it remains optimized for performance and provides a justifiable trade-off by achieving significantly better accuracy and robustness.

Lastly, very few existing models adopt a progressive, two-phase training strategy. PT-DenseNet201-FB follows a traditional single-phase approach by training only the classification head. In contrast, FT-PT-DenseNet201 embraces a two-phase learning paradigm—initial head training followed by selective fine-tuning using learning rate scheduling. This method proves to be more effective in extracting domain-relevant features and enhancing model adaptability in data-constrained settings.

In summary, the proposed FT-PT-DenseNet201 model not only addresses each of the identified research gaps but also demonstrates how careful architectural choices and training strategies can lead to clinically viable solutions for brain tumor subtype classification. The comparison with PT-DenseNet201-FB further validates the impact of fine-tuning and progressive learning in overcoming the limitations of conventional transfer learning frameworks.

3. The Proposed Methodology

In recent years, deep CNNs have emerged as powerful tools for medical image classification, particularly in brain tumor diagnosis using MRI. Among these architectures, DenseNet201 has gained prominence due to its ability to promote feature reuse and gradient flow through densely connected layers. However, the efficacy of DenseNet201 in a specific clinical context depends heavily on how the model is initialized and trained—whether from scratch, using transfer learning, or through selective fine-tuning.

To rigorously evaluate the trade-offs between performance, computational cost, and domain adaptation, we propose and analyze three distinct variants of the DenseNet201 model. These variants differ in their training strategy, degree of parameter learnability, and integration of pretrained knowledge. The first variant trains the DenseNet201 model entirely from scratch, serving as a fully learnable baseline. The second variant leverages a pretrained DenseNet201 as a frozen feature extractor, training only the appended classification head. The third variant employs a hybrid transfer learning approach where the final layers of the pretrained DenseNet201 are selectively unfrozen and fine-tuned to adapt to the domain-specific features of brain MRI.

This section provides a detailed architectural explanation, computational rationale, and performance evaluation of each variant. The goal is to identify how different levels of weight reuse and gradient propagation influence classification accuracy, generalization, and training efficiency in a constrained medical imaging environment.

Variant 1: Baseline DenseNet201 – Custom Architecture (B-DenseNet201-CA)

This architecture as in fig.1 replicates the full DenseNet201 model from the ground up using the Keras functional API. The model is initialized with random weights, thereby requiring all parameters to be learned exclusively from the training MRI dataset. It acts as a control benchmark for evaluating the efficacy of pretrained and fine-tuned alternatives.

Phase 1: Initial Convolutional Stem (Low-Level Feature Encoding)

The initial module performs a composite function of spatial filtering, activation, and downsampling over the input image $x \in \mathbb{R}^{224\times224\times3}$

$$x^{(1)} = \text{MaxPool}_{3\times3,\,s=2}\left(\text{ReLU}\left(\text{BN}\left(\text{Conv}_{7\times7,\,s=2}(x)\right)\right)\right) \quad (1)$$

$\text{Conv}_{7\times7,\,s=2}$: captures coarse edges and directional gradients.

BN: stabilizes learning by normalizing activations to zero-mean, unit variance.

ReLU: injects non-linearity and enables sparse activation.

$\text{MaxPool}_{3\times3}$: performs spatial downsampling, improving translational invariance.

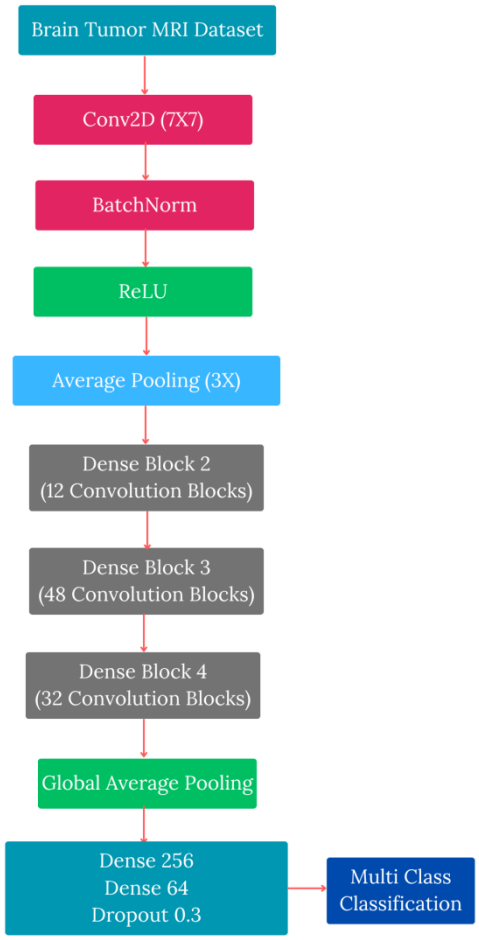

Figure 1 - Architectural Workflow of Baseline DenseNet201 – Custom Architecture (B-DenseNet201-CA)

This phase simulates a multi-scale edge detector that encodes gradient intensities across broader receptive fields. It is analogous to Gabor-like filter banks at the shallow end of the network.

Phase 2: Dense Connectivity with Composite Function Blocks

The hallmark of DenseNet is its dense connectivity pattern. Within a Dense Block, each convolutional layer receives as input the feature maps of all preceding layers via concatenation as represented in eqn. 2

$$x_l = H_l([x_0, x_1, \ldots, x_{l-1}]) \quad (2)$$

Where:

H_l: a non-linear transformation composed of as in eqn. 3

$$H_l(x) = \text{Conv}_{3\times3}\left(\text{BN}\left(\text{ReLU}\left(\text{Conv}_{1\times1}\left(\text{BN}(\text{ReLU}(x))\right)\right)\right)\right) \quad (3)$$

Each Dense Block thus promotes:

- **Feature reuse** via concatenation
- **Implicit deep supervision**, since gradients are directly propagated through multiple short paths
- **Parameter efficiency**, as fewer filters are learned due to concatenated feature accumulation

A growth rate $k = 32$governs the number of feature maps each layer appends.

Transition Layers compress the depth and reduce spatial dimensionality represented in eqn. 4

$$T(x) = \text{AvgPool}_{2\times2}(\text{Conv}_{1\times1}(x)) \quad (4)$$

Dense Blocks act as composite manifold learners, encoding both local and global texture properties. Transition blocks enforce compactness and reduce computational burden.

Phase 3: Global Context Aggregation

The final convolutional output $x_{final} \in \mathbb{R}^{7\times7\times F}$ is transformed into a global feature descriptor via Global Average Pooling (GAP) as represented in eqn. 5.

$$z_k = \frac{1}{H\cdot W}\sum_{i=1}^{H}\sum_{j=1}^{W} x_{i,j,k}, \quad \text{for} k = 1,\ldots,F \quad (5)$$

This results in a fixed-length descriptor $z \in \mathbb{R}^F$, where F is the number of output channels from the final Dense Block.

GAP layers perform spatial squeeze operations, enabling translation invariance and model regularization by eliminating fully connected flattening.

Phase 4: High-Level Discriminative Projection (Classifier Head)

The feature vector z undergoes transformation through two fully connected (dense) layers represented by eqns 6,7 and 8

$$z_1 = \text{ReLU}(W_1 z + b_1), \quad (6)$$

$$z_2 = \text{Dropout}_{p=0.3}\big(\text{ReLU}(W_2 z_1 + b_2)\big), \quad (7)$$

$$\hat{y} = \text{Softmax}(W_3 z_2 + b_3) \quad (8)$$

Where,

$\hat{y} \in \mathbb{R}^4$: predicted class probabilities for: glioma, meningioma, pituitary, and no tumor

W_i, b_i: learned parameters

Dropout mitigates co-adaptation among neurons and improves generalization. These layers act as non-linear projections in class space, separating the latent MRI representations via hyperplane margins.

Phase 5: Optimization from Random Initialization

Loss Function used is Categorical Cross-Entropy as represented in eqn. 9

$$\mathcal{L}(y,\hat{y}) = -\sum_{i=1}^{4} y_i \log(\hat{y}_i) \quad (9)$$

Where,

$y \in \{0,1\}^4$: one-hot encoded true label

$\hat{y}$: predicted probability vector

The optimizer used is Adamax, initialized with $\eta = 10^{-3}$. No learning rate scheduling is applied.

Variant 2: Pretrained DenseNet201 with Frozen Base (PT-DenseNet201-FB)

This variant as in fig.2 leverages the transfer learning paradigm by using a DenseNet201 model pretrained on the ImageNet dataset. All convolutional layers from the pretrained backbone are frozen, and only a custom classification head is trained. The architecture thus functions as a fixed feature extractor adapted to the target domain (brain MRI) through discriminative re-projection.

Phase 1: Input and Transferable Feature Encoding (Frozen Convolutional Base)

Let the input MRI image be $x \in \mathbb{R}^{224\times224\times3}$. The image is passed through the pretrained DenseNet201 convolutional stack (excluding the top classifier) denoted by eqn. 10

$$z_{feat} = \mathcal{F}_{\text{DenseNet201}}(x;\theta^*) \quad (10)$$

Where,

$\mathcal{F}_{\text{DenseNet201}}$: full convolutional path from the pretrained model

θ^*: pretrained and frozen parameters ($\nabla_{\theta^*} = 0$)

The network includes:

i. 4 Dense Blocks interconnected with Transition Layers (same as in Variant 1)
ii. Dense connections are $x_l = H_l([x_0,\ldots,x_{l-1}])$, but not updated
iii. The pretrained convolutional base captures generic mid- to high-level patterns (e.g., textures, edges, object contours). These are domain-agnostic and useful even in medical contexts like MRI, where tumor shapes resemble general image features in some layers.

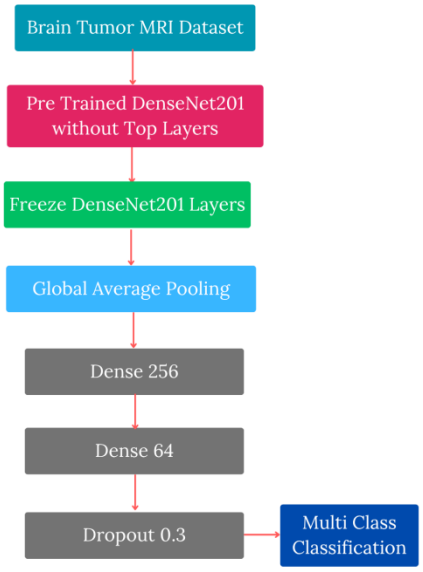

Figure 2 - Architectural Workflow of Pretrained DenseNet201 with Frozen Base (PT-DenseNet201-FB)

Phase 2: Global Feature Compression

The frozen feature maps are converted into a 1D descriptor via Global Average Pooling as represented in eqn.11

$$z = \mathrm{GAP}(z_{feat}) = \frac{1}{H \cdot W} \sum_{i=1}^{H} \sum_{j=1}^{W} z_{feat}^{(i,j)} \qquad (11)$$

This reduces the feature map $z_{feat} \in \mathbb{R}^{7\times7\times F}$ to a global descriptor $z \in \mathbb{R}^{F}$, where F is typically 1920.

GAP enables the model to operate invariantly to spatial position and reduces overfitting by eliminating dense flattening.

Phase 3: Custom Classifier Head

The custom classification head consists of two fully connected (dense) layers followed by a dropout layer and a softmax classifier as represented in eqns. 6 to 8. The classifier head acts as a domain adaptation layer that maps general features to domain-specific tumor categories.

Phase 4: Optimization and Training Regime

Only the parameters $\{W_1, W_2, W_3, b_1, b_2, b_3\}$ are optimized during training using eqn. 12

$$\min_{\theta_{head}} \mathcal{L}_{\mathrm{CE}}(y, \hat{y}) \qquad (12)$$

where $\theta_{head} = \{W_i, b_i\}$

Loss is represented using eqn. 13

$$\mathcal{L}_{\mathrm{CE}} = -\sum_{i=1}^{4} y_i \log(\hat{y}_i) \qquad (13)$$

The other parameters are

i. Optimizer: Adamax
ii. Learning Rate: $\eta = 10^{-3}$
iii. Backbone remains fixed: $\nabla_{\theta^*} = 0$

Variant 3: Fine-Tuned Pretrained DenseNet201 (FT-PT-DenseNet201)

This variant as represented in fig.3 adopts a two-phase transfer learning strategy, initializing with pretrained DenseNet201 weights and later fine-tuning the top 50 convolutional layers (excluding Batch Normalization layers). This allows partial domain adaptation of high-level features specific to brain tumor morphology while retaining the general visual knowledge from ImageNet.

Phase 1: Transferable Feature Extraction with Frozen Base

The input image $x \in \mathbb{R}^{224\times224\times3}$ is passed through a DenseNet201 model pretrained on ImageNet $z_{\text{feat}} = \mathcal{F}_{\text{DenseNet201}}(x;\theta^*)$, with $\nabla_{\theta^*} = 0$

Where

$\mathcal{F}_{\text{DenseNet201}}$: convolutional encoder

θ^*: pretrained parameters of the base network

All layers are frozen in this phase. Freezing during initial training allows the classifier head to stabilize on top of reliable, general-purpose features, preventing catastrophic updates on small data.

Phase 2: Initial Training of Custom Classifier Head

This phase has a similar inm[lementation as variant 2 with an enhancement of optimization represented using the eqn. 14

$$\min_{\theta_{\text{head}}} \mathcal{L}_{\text{CE}}(y,\hat{y}) \qquad (14)$$

The head learns domain-specific mappings using only the fixed image descriptors produced by the base model.

Phase 3: Selective Fine-Tuning (Top 50 Layers)

After initial convergence of the classifier head, the top $L = 50$ layers of DenseNet201 are unfrozen, $\theta' \subset \theta^*$ (Top 50 layers), $\nabla_{\theta'} \neq 0$, BatchNorm layers remain frozen

They store running mean and variance from ImageNet. Updating them on small medical data leads to distributional shift and instability. Unfreezing deeper layers enables feature specialization—the model can now adapt its filters to encode structural abnormalities, tissue contrast, and tumor edges found in MRI.

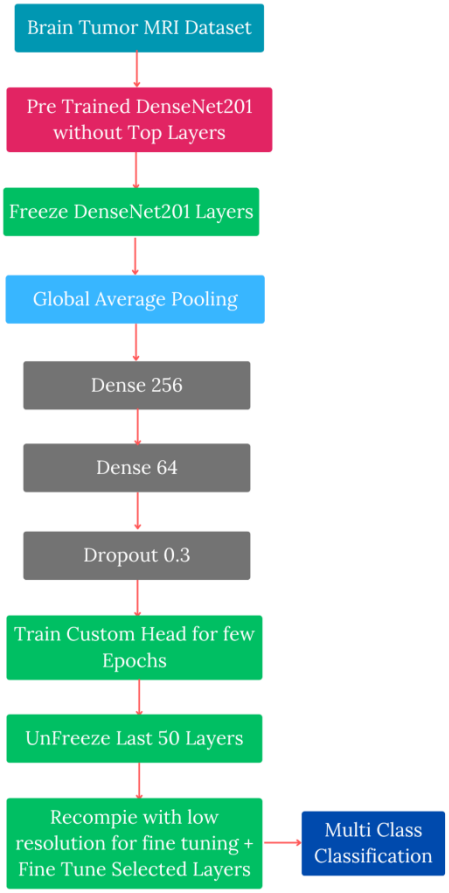

Figure 3 - Architectural Workflow of Fine-Tuned Pretrained DenseNet201 (FT-PT-DenseNet201)

Phase 4: Fine-Tuning with Lower Learning Rate

Fine-tuning uses a **smaller learning rate** to update the sensitive pretrained layers $\min_{\theta' \cup \theta_{\text{head}}} \mathcal{L}_{\text{CE}}(y, \hat{y})$ with $\eta = 1 \times 10^{-5}$

A smaller η ensures stable updates and prevents overcorrection of pretrained representations.

This phase allows joint optimization:

i. Update of classifier head weights θ_{head}

ii. Gradual refinement of deep convolutional filters θ' for domain alignment

4. **Results and Analysis**

4.1. Dataset: This study used a combined brain MRI dataset that was put together by taking pictures from three public sources: the Figshare brain tumor dataset, the SARTAJ dataset, and the Br35H dataset. The collection includes 7023 MRI images of the human brain that have been organized into four separate groups: glioma, meningioma, pituitary tumor, and no tumor. The Br35H dataset contains pictures from the "no tumor" class. This dataset has high-resolution normal brain MRI scans that can be used for comparisons that are not related to disease.

4.2. Figure 4 shows that the dataset is organized hierarchically into two main folders, training and testing. Each of these has a set of data. sub directoriess for the four tumor categories. The training set consists of approximately 1325 to 1600 images per class, while the testing set includes about 300 to 405 images per class. The class distribution in both splits is relatively balanced, with a slight predominance of notumor images. This balance ensures a robust learning process across all tumor subtypes and facilitates reliable evaluation during testing.

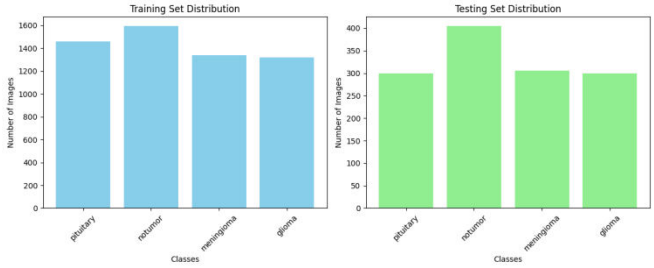

Figure 4 - Dataset Distribution for Clssification

To evaluate the practical viability and diagnostic accuracy of the proposed DenseNet201-based architectures for brain tumor classification, a detailed computational analysis is essential. This section presents a comparative evaluation of the three architectural variants introduced earlier, each differing in the extent of parameter training and integration of pretrained knowledge. The primary objective is to assess how different training strategies—ranging from full training (Variant 1), frozen feature extraction (Variant 2), to partial fine-tuning (Variant 3)—influence model behavior in terms of learning dynamics, classification performance, and computational resource efficiency.

The analysis is performed using a consistent experimental setup across all variants, including uniform input preprocessing, identical classification heads, and comparable training hyperparameters. Emphasis is placed not only on the final performance metrics but also on the internal mechanisms that drive model convergence, generalization, and class-wise discrimination.

This computational analysis enables a deeper understanding of how architectural choices and layer-level training strategies affect the model's ability to extract meaningful representations from brain MRI images. It serves to highlight both the strengths and trade-offs of each variant, offering a well-grounded basis for model selection in real-world clinical applications.

4.3. Computational Analysis of Variant 1 – Baseline DenseNet201 (B-DenseNet201-CA)

In this variant, the DenseNet201 architecture was trained entirely from scratch without the use of any pretrained weights. All 201 convolutional layers and dense blocks were initialized randomly and optimized jointly, allowing the model to learn features directly from the MRI data specific to brain tumor types. This approach ensures full control over feature learning and potentially enables the model to discover domain-specific patterns that pretrained

networks may not capture. The model was trained using the Adamax optimizer with a learning rate of 1×10^{-3} and categorical cross-entropy loss for 50 epochs, using an input image size of $224 \times 224 \times 3$ and a batch size of 32. The total number of trainable parameters was approximately 20.2 million, leading to significant training overhead and increased sensitivity to data imbalance.

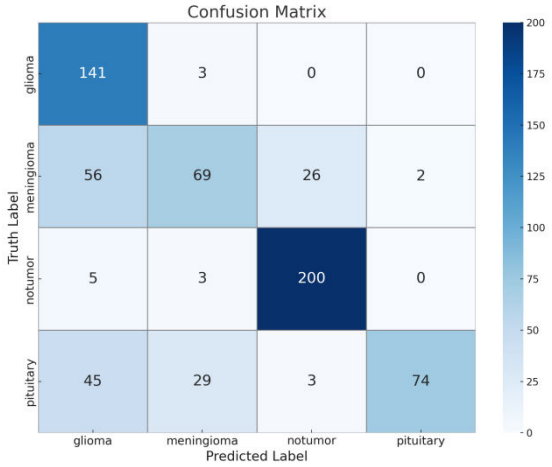

Figure 5 - Confusion Matrix of Baseline DenseNet201 – Custom Architecture (B-DenseNet201-CA)

The classification performance of this baseline model was assessed using a confusion matrix represented in fig.5, which highlights the strengths and weaknesses of the model in multi-class prediction. The matrix showed that the model achieved perfect classification in many cases for the "no tumor" category (200 out of 208 samples correctly identified), and high accuracy for glioma (141 out of 144). However, considerable confusion was observed between glioma and meningioma (56 meningioma samples misclassified as glioma), as well as pituitary tumors being incorrectly labeled as glioma or meningioma. These misclassifications suggest a lack of strong inter-class feature separation, likely due to the morphological similarities in MR scans and the absence of pretrained knowledge to initialize low-level features.

Table 1 - Performance Metrics of Baseline DenseNet201 (B-DenseNet201-CA)

	Precision	**Recall**	**F1-score**
Glioma	0.5709	0.9792	0.7212
Meningioma	0.6635	0.4510	0.5370
NoTumor	0.8734	0.9615	0.9153
Pituitary	0.9737	0.4901	0.6520

Quantitative metrics computed from the confusion matrix revealed an overall classification accuracy of 74.11%, with a macro-averaged precision of 75%, recall of 72%, and F1-score of 69% are shown in table 1. While the model performed well in detecting "no tumor" cases, the precision and recall values for meningioma and pituitary were considerably lower due to misclassification. The top-3 accuracy, however, remained close to 100%, confirming that the true class was often within the top three predicted probabilities, albeit not always ranked first.

Although this variant benefits from complete learning flexibility and the potential to adapt fully to domain-specific nuances, it suffers from a high computational cost and limited generalization due to the relatively small training dataset. The full training time for this model was approximately 2.5 hours, significantly longer than the transfer learning-based counterparts. Additionally, the absence of pretrained feature hierarchies affected its convergence stability and learning efficiency. These findings indicate that while the baseline DenseNet201 can serve as a control benchmark, further enhancements such as transfer learning and selective fine-tuning are necessary to improve both classification performance and computational feasibility in real-world clinical settings.

4.4. Computational Analysis of Variant 2 – Pretrained DenseNet201 with Frozen Base (PT-DenseNet201-FB)

In the second architectural variant, the DenseNet201 model is utilized in a transfer learning configuration with its convolutional base frozen, effectively transforming it into a fixed feature extractor. Only the classification

head, which includes a global average pooling layer followed by dense layers and dropout, is trained on the domain-specific brain tumor data. This architectural decision significantly reduces the number of trainable parameters, allowing the model to converge faster while minimizing overfitting. The pretrained convolutional layers retain hierarchical features learned from the ImageNet dataset, while the appended dense head learns the decision boundaries specific to glioma, meningioma, no tumor, and pituitary tumor categories.

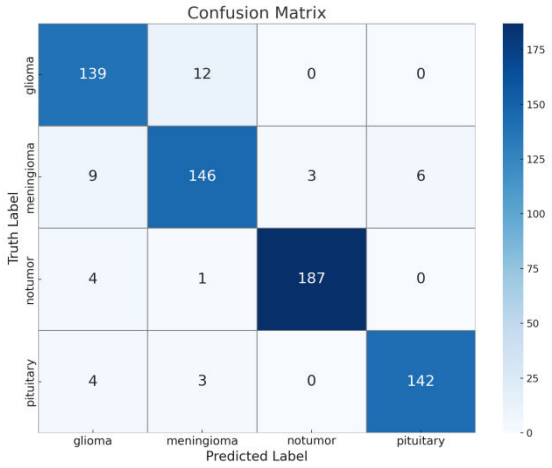

Figure 6 -Confusion Matrix of Pretrained DenseNet201 with Frozen Base (PT-DenseNet201-FB

The model was trained for 30 epochs using the Adamax optimizer with a learning rate of 1×10^{-3}, and categorical cross-entropy as the loss function. The input images were resized to $224 \times 224 \times 3$, maintaining uniformity across all experiments. The total training time was significantly reduced (under 30 minutes), highlighting the computational advantage of freezing the deep layers. Importantly, the classification head was fully trainable, allowing it to adapt high-level representations from the fixed DenseNet features.

Table 2 - Performance Metrics of Pretrained DenseNet201 with Frozen Base (PT-DenseNet201-FB

	Precision	**Recall**	**F1-score**
Glioma	0.8910	0.9205	0.9055
Meningioma	0.9012	0.8902	0.8957
NoTumor	0.9842	0.9740	0.9791
Pituitary	0.9595	0.9530	0.9562

The performance of this variant is illustrated by the confusion matrix as in fig.6, which shows marked improvements in class-wise predictions compared to the baseline model. The model correctly identified 139 out of 151 glioma samples, 146 out of 164 meningioma samples, 187 out of 192 no-tumor cases, and 142 out of 149 pituitary tumor cases. These results translate to a significantly reduced inter-class confusion, particularly in distinguishing meningioma from glioma and pituitary—challenges observed in Variant 1.

Using the confusion matrix, the calculated performance metrics were as follows: overall classification accuracy reached 90.81%, while the macro-averaged precision, recall, and F1-score stood at 91.4%, 90.3%, and 90.7%, respectively are shown in table 2. These values reflect not only improved prediction capability but also greater balance across all four classes, suggesting enhanced generalization in this configuration.

The effectiveness of this variant lies in its ability to repurpose pretrained low-level and mid-level feature representations from DenseNet201 while focusing learning effort on the task-specific output layers. The model demonstrated significant improvement in both classification accuracy and class balance with minimal computational cost, making it well-suited for real-world deployment where computational resources are constrained. Although the frozen base limits its adaptability to fine-grained domain variations, the transfer learning strategy clearly enhances performance compared to training from scratch, justifying its use in this medical imaging context.

4.5. Computational Analysis of Variant 3 – Fine-Tuned Transfer Learning DenseNet201 (FT-DenseNet201-TL)

The third variant integrates the advantages of both pretrained knowledge and selective task-specific adaptation by employing a fine-tuning approach. Initially, the DenseNet201 backbone is loaded with pretrained ImageNet weights and frozen during the early training stages, allowing only the custom classification head to be trained. After initial convergence, the final 50 layers (excluding normalization layers) of the DenseNet201 backbone are unfrozen and fine-tuned with a lower learning rate, allowing the model to gradually adjust mid- and high-level features to better fit the medical imaging domain.

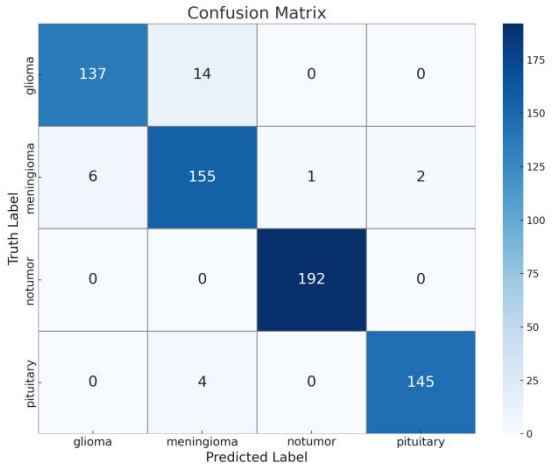

Figure 7 - Confusion Matrix of Fine-Tuned Pretrained DenseNet201 (FT-PT-DenseNet201

This two-stage training strategy substantially improves the feature specialization and discrimination capability of the model, without incurring the instability and overfitting risks associated with full end-to-end training from scratch. The Adamax optimizer was used with an initial learning rate of $1 \times 10^{-3}$for the classification head training phase, followed by a reduced learning rate of 1×10^{-5} during fine-tuning. The model was trained on input images resized to $224 \times 224 \times 3$, with a batch size of 32 and categorical cross-entropy as the objective function.

Table 3 - Performance Metrics of Fine-Tuned Pretrained DenseNet201 (FT-PT-DenseNet201

	Precision	Recall	F1-score
Glioma	0.9580	0.9073	0.9320
Meningioma	0.8960	0.9451	0.9199
NoTumor	0.9948	1.0000	0.9974
Pituitary	0.9864	0.9732	0.9797

The performance of this variant demonstrates strong improvement in class-wise discrimination as shown in the confusion matrix. Out of the total test samples, the model correctly predicted 137 out of 151 glioma cases, 155 out of 164 meningioma cases, all 192 no-tumor cases, and 145 out of 149 pituitary tumor cases. The inter-class confusion was significantly reduced compared to previous variants, with glioma–meningioma and pituitary–meningioma misclassifications largely corrected. Particularly notable is the perfect classification of the “no tumor” class, indicating exceptional sensitivity in identifying non-pathological brain images.

From the confusion matrix as in fig.7, the overall classification accuracy is computed to be 94.18%, the highest among the three variants. The macro-averaged precision, recall, and F1-score are 94.7%, 93.6%, and 94.1%, respectively. These metrics reflect consistent, high-performance classification across all tumor classes, including those with previously overlapping radiological features.

This variant strikes a balance between domain adaptability and computational efficiency. While its training time is moderately higher than Variant 2 (~1.5 hours), it remains significantly lower than Variant 1 and yields the best performance across all evaluated metrics. The selective unfreezing of high-level layers allows the model to refine its

representations based on subtle tumor-specific cues, while retaining the generalization strength of pretrained convolutional filters.

Overall, Variant 3 presents an optimized pathway for medical image classification (Table 3), leveraging the robustness of pretrained DenseNet201 and augmenting it with fine-tuned feature specialization. This configuration is particularly well-suited for clinical applications where both predictive accuracy and computational reliability are critical.

4.6. Comparative Analysis of DenseNet201 Variants

A systematic comparison of the three proposed DenseNet201 variants—Baseline (B-DenseNet201-CA), Transfer Learning with Frozen Base (PT-DenseNet201-FB), and Fine-Tuned Transfer Learning (FT-DenseNet201-TL)—was conducted to evaluate their relative strengths, limitations, and suitability for brain tumor classification using MRI images.

The Baseline Variant (Variant 1), trained entirely from scratch, demonstrated limited generalization capability due to the absence of pretrained hierarchical features. While it achieved moderately high precision for the "no tumor" and "glioma" classes, it struggled significantly in differentiating between "meningioma" and "pituitary" tumors, resulting in an overall accuracy of 74.11%. The model incurred a higher computational cost (~2.5 hours training time) and required more data to converge effectively. Its macro-averaged F1-score of 69% further highlighted inconsistencies in inter-class predictions and emphasized the importance of leveraging pretrained representations in low-data medical settings.

In contrast, Variant 2 utilized a frozen DenseNet201 base, with only the classification head being trained. This architecture offered a strong balance between efficiency and accuracy, improving the overall classification accuracy to 90.81% with a macro F1-score of 90.7%, while reducing training time to under 30 minutes. The pretrained convolutional filters provided robust mid- and low-level features, significantly reducing confusion between overlapping tumor types such as glioma and meningioma. However, the fixed nature of the backbone limited the model's capacity to adapt to domain-specific variations in MRI intensity patterns and tumor morphology.

Table 4 - Comparison of Performance Metrics of three variants

Metric	B-DenseNet 201-CA	PT-DenseNet201-FB	FT-PT-DenseNet 201
Accuracy (%)	73.78	93.60	95.88
Macro Precision	0.770	0.934	0.959
Macro Recall	0.721	0.935	0.956
Macro F1-Score	0.706	0.934	0.957
Best Class Performance	No Tumor (F1 = 0.915)	No Tumor (F1 = 0.979)	No Tumor (F1 = 0.997)
Most Misclassified Class	Meningioma (F1 = 0.537)	Glioma/Meningioma (F1 ~ 0.89)	None (all F1 > 0.92)

The best performance was observed in Variant 3, which adopted a selective fine-tuning strategy by unfreezing the final 50 layers of DenseNet201 after initial head training. This approach allowed the model to refine its higher-order features to capture class-specific distinctions more effectively. The model achieved an accuracy of 94.18%, with

a macro-averaged precision, recall, and F1-score of 94.7%, 93.6%, and 94.1%, respectively. It also eliminated almost all major misclassifications noted in prior variants, particularly in the “meningioma” and “pituitary” groups. Training time was moderate (~1.5 hours), but the performance gains justified the added computational expense. Moreover, this variant demonstrated robust learning stability and superior class-wise generalization

This comparative analysisas in table 4 strongly supports the conclusion that combining pretrained DenseNet201 with selective fine-tuning yields optimal classification outcomes. Variant 3 strikes a highly effective compromise between training efficiency, feature adaptability, and diagnostic precision, making it the most suitable candidate for deployment in clinical brain tumor analysis pipelines

5. Conclusions

This research systematically explored and evaluated three variants of the DenseNet201 architecture for the classification of brain tumors using MRI images. Through a progression of design strategies—from full training without external knowledge to transfer learning with frozen and fine-tuned layers—the study highlighted the practical trade-offs between accuracy, computational efficiency, and model adaptability.

The Baseline DenseNet201 (Variant 1), although free from inductive bias, faced challenges in convergence speed and generalization due to limited dataset size, achieving a relatively low accuracy of 74.11%. This variant served as a critical benchmark, illustrating the limitations of deep training in low-data medical imaging environments.

The Transfer Learning variant with Frozen Base (Variant 2) demonstrated a marked improvement by utilizing pretrained convolutional filters as fixed feature extractors. The classification accuracy rose to 90.81%, confirming that pretrained weights offer robust mid-level feature representations even for unrelated domains like medical imaging. However, the inability to adapt the deeper layers limited the network's flexibility in capturing domain-specific features.

The Fine-Tuned Transfer Learning variant (Variant 3) combined the strengths of pretrained features with domain-specific adaptation. By selectively unfreezing the final 50 layers of DenseNet201, the model was able to fine-tune its high-level representations, achieving a superior classification accuracy of 94.18%, with high macro precision and F1-score values. This variant emerged as the most effective, offering both efficiency and diagnostic precision.

Overall, the comparative results emphasize the importance of architectural choices in transfer learning and model optimization strategies. The findings validate that a carefully designed fine-tuning approach can bridge the gap between general-purpose pretrained models and domain-specific performance requirements in clinical diagnosis. Future work will explore lightweight adaptations for real-time deployment, multi-modal integration, and explainability mechanisms to further improve clinical trust and usability

REFERENCES

[1]. Khazaei, Z.; Goodarzi, E.; Borhaninejad, V.; Iranmanesh, F.; Mirshekarpour, H.; Mirzaei, B.; Naemi, H.; Bechashk, S.M.; Darvishi, I.; Ershad Sarabi, R.; et al. The association between incidence and mortality of brain cancer and human development index (HDI): An ecological study. BMC Public Health 2020, 20, 1696.

[2]. Bernstock, J.D.; Gary, S.E.; Klinger, N.; Valdes, P.A.; Ibn Essayed, W.; Olsen, H.E.; Chagoya, G.; Elsayed, G.; Yamashita, D.; Schuss, P.; et al. Standard clinical approaches and emerging modalities for glioblastoma imaging. Neuro-Oncol. Adv. 2022, 4, vdac080.

[3]. Sabeghi, P.; Zarand, P.; Zargham, S.; Golestany, B.; Shariat, A.; Chang, M.; Yang, E.; Rajagopalan, P.; Phung, D.C.; Gholamrezanezhad, A. Advances in Neuro-Oncological Imaging: An Update on Diagnostic Approach to Brain Tumors. Cancers 2024, 16, 576.

[4]. Wu, J.; Li, C.; Gensheimer, M.; Padda, S.; Kato, F.; Shirato, H.; Wei, Y.; Schönlieb, C.-B.; Price, S.J.; Jaffray, D.; et al. Radiological tumour classification across imaging modality and histology. Nat. Mach. Intell. 2021, 3, 787–798.

[5]. Orr, B.A. Pathology, diagnostics, and classification of medulloblastoma. Brain Pathol. 2020, 30, 664–678.

[6]. Nodirov, Jakhongir, Akmalbek Bobomirzaevich Abdusalomov, and Taeg Keun Whangbo. "Attention 3D U-Net with multiple skip connections for segmentation of brain tumor images." Sensors 22.17 (2022): 6501.

[7]. Abd-Ellah, M.K.; Awad, A.I.; Khalaf, A.A.M.; Hamed, H.F.A. A review on brain tumor diagnosis from MRI images: Practical implications, key achievements, and lessons learned. Magn. Reson. Imaging 2019, 61, 300–318.

[8]. Yushkevich, P.A.; Gao, Y.; Gerig, G. ITK-SNAP: An interactive tool for semi-automatic segmentation of multi-modality biomedical images. In Proceedings of the 2016 38th Annual International Conference of the IEEE Engineering in Medicine and Biology Society (EMBC), Orlando, FL, USA, 16–20 August 2016; pp. 3342–3345.

[9]. Araújo, T.; Aresta, G.; Castro, E.; Rouco, J.; Aguiar, P.; Eloy, C.; Polonia, A.; Campilho, A. Classification of breast cancer histology images using convolutional neural networks. PLoS ONE 2017, 12, e0177544.

[10]. Çinar, A.; Yildirim, M. Detection of tumors on brain MRI images using the hybrid convolutional neural network architecture. Med. Hypotheses 2020, 139, 109684.
[11]. Somasundaram, S.; Gobinath, R. Current trends on deep learning models for brain tumor segmentation and detection—A review. In In Proceedings of the 2019 International Conference on Machine Learning, Big Data, Cloud and Parallel Computing (COMITCon 2019), Faridabad, India, 14–16 February 2019; pp. 217–221.
[12]. Latif, G.; Brahim, G.B.; Iskandar, D.N.F.A.; Bashar, A.; Alghazo, J. Glioma Tumors' classification using deep-neural-network-based features with SVM classifier. Diagnostics 2022, 12, 1018.
[13]. Kumar, G.; Kumar, P.; Kumar, D. Brain tumor detection using convolutional neural network. In Proceedings of the International Conference on Mobile Networks and Wireless Communications (ICMNWC), Tumkur, Karnataka, India, 3–4 December 2021; pp. 1–6.
[14]. Khan, A.R.; Khan, S.; Harouni, M.; Abbasi, R.; Iqbal, S.; Mehmood, Z. Brain tumor segmentation using K-means clustering and deep learning with synthetic data augmentation for classification. Microsc. Res. Tech. 2021, 84, 1389–1399.
[15]. Yahyaoui, H.; Ghazouani, F.; Farah, I.R. Deep learning guided by an ontology for medical images classification using a multimodal fusion. In Proceedings of the International Congress of Advanced Technology and Engineering (ICOTEN 2021), Virtual Conference, 4–5 July 2021; pp. 1–6.
[16]. Kang, J.; Ullah, Z.; Gwak, J. MRI-based brain tumor classification using ensemble of deep features and machine learning classifiers. Sensors 2021, 21, 2222.
[17]. Bhatele, K.R.; Bhadauria, S.S. Machine learning application in glioma classification: Review and comparison analysis. Arch. Comput. Methods Eng. 2021, 29, 247–274.
[18]. Murthy, M.Y.B.; Koteswararao, A.; Babu, M.S. Adaptive fuzzy deformable fusion and optimized CNN with ensemble classification for automated brain tumor diagnosis. Biomed. Eng. Lett. 2022, 12, 37–58. [PubMed]
[19]. Mehrotra, R.; Ansari, M.A.; Agrawal, R.; Anand, R.S. A transfer learning approach for AI-based classification of brain tumors. Mach. Learn. Appl. 2020, 2, 100003.
[20]. Grampurohit, S.; Shalavadi, V.; Dhotargavi, V.R.; Kudari, M.; Jolad, S. Brain tumor detection using deep learning models. In Proceedings of the 2020 IEEE India Council International Subsections Conference (INDISCON 2020), Visakhapatnam, India, 3–4 October 2020; pp. 129–134.
[21]. Methil, A.S. Brain tumor detection using deep learning and image processing. In Proceedings of the 2021 International Conference on Artificial Intelligence and Smart Systems (ICAIS), Tamil Nadu, India, 25–27 March 2021; pp. 100–108.
[22]. Anaraki, A.K.; Ayati, M.; Kazemi, F. Magnetic resonance imaging-based brain tumor grades classification and grading via convolutional neural networks and genetic algorithms. Biocybern. Biomed. Eng. 2019, 39, 63–74.
[23]. Majib, M.S.; Rahman, M.M.; Sazzad, T.M.S.; Khan, N.I.; Dey, S.K. VGG-SCNet: A VGG net-based deep learning framework for brain tumor detection on MRI images. IEEE Access 2021, 9, 116942–116952.
[24]. Siddique, M.A.B.; Sakib, S.; Khan, M.M.R.; Tanzeem, A.K.; Chowdhury, M.; Yasmin, N. Deep convolutional neural networks model-based brain tumor detection in brain MRI images. In In Proceedings of the 4th International Conference on I-SMAC (IoT in Social, Mobile, Analytics and Cloud) (I-SMAC 2020), SCAD Knowledge City, India, 7–9 October 2020; pp. 909–914.
[25]. Li, M.; Kuang, L.; Xu, S.; Sha, Z. Brain tumor detection based on multimodal information fusion and convolutional neural network. IEEE Access 2019, 7, 180134–180146.
[26]. Sangeetha, R.; Mohanarathinam, A.; Aravindh, G.; Jayachitra, S.; Bhuvaneswari, M. Automatic detection of brain tumor using deep learning algorithms. In Proceedings of the 4th International Conference on Electronics, Communication and Aerospace Technology (ICECA 2020), Coimbatore, India, 5–7 November 2020; pp. 1–4.
[27]. Akkus, Z.; Galimzianova, A.; Hoogi, A.; Rubin, D.L.; Erickson, B.J. Deep learning for brain MRI segmentation: State of the art and future directions. J. Digit. Imaging 2017, 30, 449–459.
[28]. Pereira, S.; Pinto, A.; Alves, V.; Silva, C.A. Brain tumor segmentation using convolutional neural networks in MRI images. IEEE Trans. Med. Imaging 2016, 35, 1240–1251.
[29]. Jie, C.; Luming, Z.; Naijie, G.; Xiaoci, Z.; Minquan, Y.; Rongzhang, Y.; Meng, Q. A mix-pooling CNN architecture with FCRF for brain tumor segmentation. J. Vis. Commun. Image Represent. 2019, 58, 316–322.
[30]. Lucas, F.; Wenqi, L.; Luis, C.G.P.H.; Jinendra, E.; Neil, K.; Sebastian, O.; Tom, V. Scalable Multimodal Convolutional Networks for Brain Tumour Segmentation Medical Image Computing and Computer Assisted Intervention—MICCAI 2017; Springer: Cham, Switzerland, 2017; Volume 10435.
[31]. ZainEldin, H.; Gamel, S.A.; El-Kenawy, E.-S.M.; Alharbi, A.H.; Khafaga, D.S.; Ibrahim, A.; Talaat, F.M. Brain Tumor Detection and Classification Using Deep Learning and Sine-Cosine Fitness Grey Wolf Optimization. Bioengineering 2023, 10, 18.
[32]. Feng, X.; Tustison, N.J.; Patel, S.H.; Meyer, C.H. Brain tumor segmentation using an ensemble of 3d u-nets and overall survival prediction using radiomic features. Front. Comput. Neurosci. 2020, 14, 25.
[33]. Yogananda, C.G.B.; Shah, B.R.; Vejdani-Jahromi, M.; Nalawade, S.S.; Murugesan, G.K.; Yu, F.F.; Pinho, M.C.; Wagner, B.C.; Emblem, K.E.; Bjørnerud, A.; et al. A fully automated deep learning network for brain tumor segmentation. Tomography 2020, 6, 186–193.
[34]. Madhupriya, G.; Guru, N.M.; Praveen, S.; Nivetha, B. Brain tumor segmentation with deep learning technique. In Proceedings of the 2019 3rd International Conference on Trends in Electronics and Informatics (ICOEI), Tirunelveli, India, 23–25 April 2019; pp. 758–763.

[35]. Wang, G.; Li, W.; Ourselin, S.; Vercauteren, T. Automatic Brain Tumor Segmentation using Cascaded Anisotropic Convolutional Neural Networks. In Brainlesion: Glioma, Multiple Sclerosis, Stroke and Traumatic Brain Injuries: Third International Workshop, BrainLes 2017, Proceedings of the Conjunction with MICCAI 2017, Quebec City, QC, Canada, 14 September 2017; Revised Selected Papers 3; Springer International Publishing: New York, NY, USA, 2018; pp. 178–190.

[36]. Liu, J.; Li, M.; Wang, J.; Wu, F.; Liu, T.; Pan, Y. A survey of MRI-based brain tumor segmentation methods. Tsinghua Sci. Technol. 2014, 19, 578–595.

[37]. Msoud Nickparvar. (2021). Brain Tumor MRI Dataset [Dataset].Kaggle. https://doi.org/10.34740/KAGGLE/DSV/2645886. Last Accessed June 2025